Research Article | Vol. 29, No. 10 / 10 May 2021 / Optics Express 15595
Optics EXPRESS

Broadband tunable orbital angular momentum mode converter based on a conventional single-mode all-fiber configuration

MIN ZHOU,[1,2] ZHE ZHANG,[2,3] LAIPENG SHAO,[2] SHEN LIU,[2,4] YU LIU,[1,5] YU PANG,[1] ZHIYONG BAI,[2] CAILING FU,[2] WEI CUI,[1] LIN QI,[1] AND YIPING WANG[2]

[1] *School of Communication and Information Engineering, Chongqing University of Posts and Telecommunications, Chongqing, 400065, China*
[2] *Key Laboratory of Optoelectronic Devices and Systems of Ministry of Education/Guangdong Province, College of Physics and Optoelectronic Engineering, Shenzhen University, Shenzhen 518060, China*
[3] *Guangdong Provincial Key Laboratory of Optical Fiber Sensing and Communication, Institute of Photonics Technology, Jinan University, Guangzhou, 511443, China*
[4] *shenliu@szu.edu.cn*
[5] *liuyu@cqupt.edu.cn*

Abstract: A broadband tunable orbital angular momentum (OAM) mode converter based on a helical long-period fiber grating (HLPFG) inscribed in a conventional single-mode fiber (SMF) is experimentally demonstrated. The proposed all-fiber OAM mode converter is based on the core-cladding mode dual resonance near the dispersion turning point (DTP). The converter can operate with a bandwidth of 303.9 nm @ −3 dB and 182.2 nm @ −10 dB, which is, as far as we know, the widest bandwidth for a conventional SMF. Furthermore, the bandwidth of the OAM mode can be dynamically tuned within a large dynamic range (>80 nm) by simply twisting the fiber clockwise (CW) or counterclockwise (CCW). The dynamic tunability of the bandwidth of the proposed OAM mode generator may find vital applications in large-capacity optical fiber communication systems.

1. Introduction

Tremendous efforts have been made in countering the optical fiber network "capacity crunch" during the past decades, such as Dense Wavelength Division Multiplexing (DWDM), Space Division Multiplexing (SDM) and Mode Division Multiplexing (MDM) techniques [1–3]. In recent years, large attentions have been drawn on orbital angular momentum (OAM) modes due to its helical phase, which can carry a lot of information in a unique dimension and thus is attractive in optical communication systems [4] as well as in other fields such as optical tweezer [5] and nanoscale microscope [6]. For OAM mode generation in free space, plenty of schemes, such as spiral phase plate [7], spatial light modulators [8], q-plate [9] and metamaterials phase plates [10] have been reported. However, additional coupling system is critical to integrate the free space OAM modes with the existing optical fiber communication systems.

All-fiber versatile OAM mode generator have been reported in recent years and the most popular is helical long-period fiber grating (HLPFG) [11–13], which possess advantages of high mode conversion efficiency, low insertion loss, and simplicity in structure. The HLPFG can be inscribed by CO_2 laser [11–18], arc discharge [19], and even oxyhydrogen-flame [20]. Various fiber types, such as conventional single-mode fibers (SMFs) [13,21], few-mode fibers (FMFs) [14–16], polarization-maintained fibers [17], as well as photonic crystal fiber (PCFs) [18] have been reported for HLPFG inscription and OAM mode generation. However, the bandwidth of

#421967
Journal © 2021
https://doi.org/10.1364/OE.421967
Received 17 Mar 2021; revised 16 Apr 2021; accepted 16 Apr 2021; published 6 May 2021

Optics EXPRESS

conventional HLPFG-based OAM converter is narrow (several tens of nanometer @−10 dB), which limits the potential wavelength multiplexing abilities.

More recently, dual resonance effect has been employed for generating broadband OAM modes. In 2019, Guo et al. reported a broadband OAM mode generator based on a dual-resonant two-mode LPFG [16], a bandwidth of 118.2 nm @ −10 dB is demonstrated. In 2020, Zhao et al. reported a CO_2-laser-inscribed dual-resonant HLPFG in a two-mode fiber, the obtained bandwidth is 297 nm @ −10 dB [15]. Compared with specific fibers, conventional SMF is more popular and compatible with the existing fiber-optic system. Although the cladding mode cannot propagate for a long distance, one can simply fusion splice it with a custom-made fiber for OAM mode transmissions. The feasibility of conventional SMF for broadband OAM generating has been theoretically demonstrated by Ren et. al. in 2020, and the obtained bandwidth is 287 nm @ −3 dB [22]. However, the experimental demonstration has not been reported as yet.

In this paper, we reported on a conventional SMF-based dual-resonance HLPFG for broadband (303.9 nm @ −3 dB and 182.2 nm @ −10 dB) tunable OAM mode generation. The oxyhydrogen-flame setup is adopted in preparing the HLPFG, which is the first experimental demonstration of SMF-based broadband OAM mode generator. The achieved OAM mode bandwidth is, as far as we know, the broadest with a conventional SMF. More importantly, the proposed OAM mode converter exhibits an excellent dynamic tunability of bandwidth, which is attractive in large-capacity optical fiber communication systems.

2. Dual-resonance principle and HLPFG preparation setup

2.1. Dual-resonant effect

In order to depict the dual-resonant principle, a Finite-Element-Method (FEM) is employed to calculate the total dispersion (including material and waveguide dispersion) of the core and several cladding modes of a conventional SMF. Within the simulation, the core/cladding diameters and the refractive index (RI) difference between the core and cladding are set as 8.2/125 µm and 0.0054, respectively. The resonant equation of a LPFG can be expressed by

$$\lambda_{res} = (n_{co}^{eff} - n_{cl,m}^{eff})\Lambda \tag{1}$$

where λ_{res} and Λ denote the resonance wavelength and grating pitch, respectively. n_{co}^{eff} and $n_{cl,m}^{eff}$ represent the effective RIs of the core and cladding modes, respectively. By taking the obtained effective RIs into Eq. (1), the resonant wavelengths of cladding modes with orders from 9 to 11 versus the grating pitch Λ is obtained and plotted in Fig. 1, where the white dots with a black edge denotes the DTP. Obviously, the DTPs represents the maximum grating pitch for each cladding mode resonance and the corresponding grating pitch of the $LP_{1,9}$, $LP_{1,10}$, $LP_{1,11}$ modes are about 172.4, 205.3, and 251.3 µm, respectively. As shown in Fig. 1, the slopes of the cladding modes $LP_{1,9}$, $LP_{1,10}$, $LP_{1,11}$ switch the signs from positive to negative with wavelength increasing, while at the DTP, $|d\lambda_{res}/d\lambda_{res}| \to \infty$. When the grating pitch is set at the DTP, there exists only one resonant dip and when the grating pitch Λ decreases, two resonant dips will arise. In special, if the grating pitch Λ is slightly smaller than the DTP, the two resonance dips can be overlapped, forming a broadband resonant dip. It is worth noting that, the two overlapped resonant dips are the same cladding mode (i.e. with the same order). As such, the broadband resonant dip has an excellent mode purity. This is the basic principle for generating broadband core-cladding modes resonance.

2.2. Oxyhydrogen-flame setup for HLPFG inscription

In addition, for generating helical phase modulation and OAM modes, the helical structure of the fiber is necessary. Figure 2(a) depicts our homemade HLPFG preparation system, where an oxyhydrogen flame is used to fuse the fiber and a rotation motor is employed to twist the

Optics EXPRESS

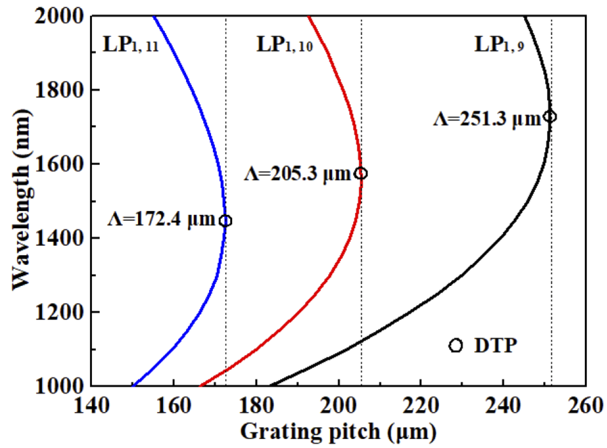

Fig. 1. Calculated resonant wavelength versus grating pitch Λ for different cladding modes (Mode orders from m = 9 to 11, the DTPs are highlighted with hollow dots with black edge.)

softened fiber, introducing helical phase modulation. In Fig. 2(a), V_1 (mm/s) and V_2 (mm/s) are the velocities of the stage-1 and stage-2, respectively. A little velocity difference between V_1 and V_2 ($V_1 < V_2$) is applied to the fiber to introduce a constant stress along the axial direction, which ensures a stretched state of the fiber. The length L of HLPFG is determined by V_2 and the time T according to

$$L = V_2 T \tag{2}$$

The grating pitch Λ can be written as

$$\Lambda = 60 V_2 / \Omega \tag{3}$$

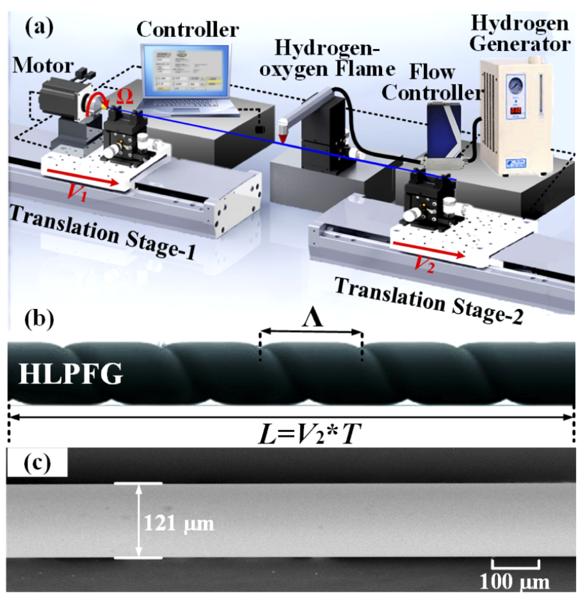

Fig. 2. (a) Schematic diagram of the homemade hydrogen-oxygen flame HLPFG preparation setup; (b) Schematic illustration of the helical modulation of the HLPFG; (c) Side view SEM image of a prepared HLPFG (i.e. S_1).

Optics EXPRESS

where Ω (rpm) is the rotation speed of the rotator. Figure 2(b) schematically illustrates the helical phase modulation of the HLPFG. By tuning the rotation rate of the motor and the translation rate of the stages, the grating pitch Λ can be precisely turned to the DTP. Scanning Electronic Microscope (SEM) image of a prepared HLPFG (S_1) at the DTP of $LP_{1,\ 10}$ mode is shown in Fig. 2(c), where the measured outer diameter of fiber (121 μm) is a little smaller than of the standard SMF (125 μm). It is worth noting that, Fig. 2(b) is merely a schematic diagram of the stress modulation of the HLPFG, in practice, the fiber shows no geometric change but thinning. As a result, no helical structure can be observed from the SEM image. Transmission spectrum of S_1 is measured and shown in Fig. 3(a), where the resonant bandwidth are 230.1 nm @ −3 dB and 145.4 nm @ −10 dB, respectively. The mode field image at the center of resonant dip (1450.0 nm) is shown in Fig. 3(b), where we can see that the excited cladding mode at ~1450.0 nm is $LP_{1,\ 10}$. As such, both the grating pitch Λ and resonant wavelength of the experiments exhibit a little deviation from the calculated results shown in Fig. 1. We believe that, the little deviation can be attributed to the thinning (from 125 to 121 μm) of the fiber during HLPFG preparation, which modifies the dispersion curve of the core and cladding modes slightly. In order to verify the helical phase of the generated $LP_{1,\ 10}$ mode, a Mach-Zehnder interferometric (MZI) system is constructed for OAM phase characterization, details of the setup are available in [13]. Figure 3(c) shows the measured OAM mode profile by the MZI system, where the order of topological charge is 1. The experimental observation convinces the efficient generation of the OAM mode by the HLPFG.

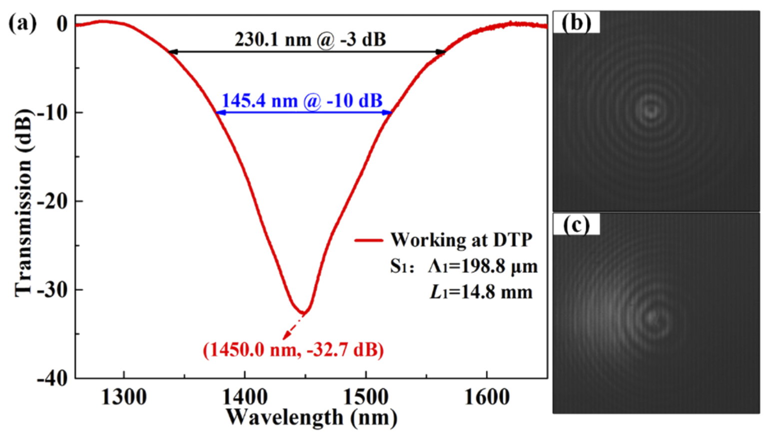

Fig. 3. (a) Transmission spectrum of a prepared HLPFG (S_1) working at the DTP. (b) Mode field profile within the center of resonant dip (i.e. 1450.0 nm); (c) OAM mode profile obtained by the MZI system.

3. Broadband HLPFG preparation and OAM mode characterization

3.1. Preparation and transmission spectra of the broadband HLPFG

We further prepare some HLPFGs (S_2-S_5) with gradually decreased grating pitch Λ to obtain a broader resonance bandwidth. Figure 4(a) depicts the transmission spectra of the five prepared HLPFGs, where the grating pitch of S_1 is at the DTP (198.8 μm) and the grating pitch of S_2 (198.3 μm), S_3 (197.9 μm), S_4 (197.5 μm), and S_5 (196.7 μm) decrease gradually. With the decreasing of grating pitch Λ, the single resonant dip splits and shifts toward the opposite directions. This observation agrees well with the calculations shown in Fig. 1. The resonant bandwidth of S_1-S_5 at −3 and −10 dB are measured and plotted in Fig. 4(b), respectively, where

Optics EXPRESS

an approximate linear relationship between the bandwidth of −3 dB and grating pitch Λ is presented, the linearities are 99.94%.

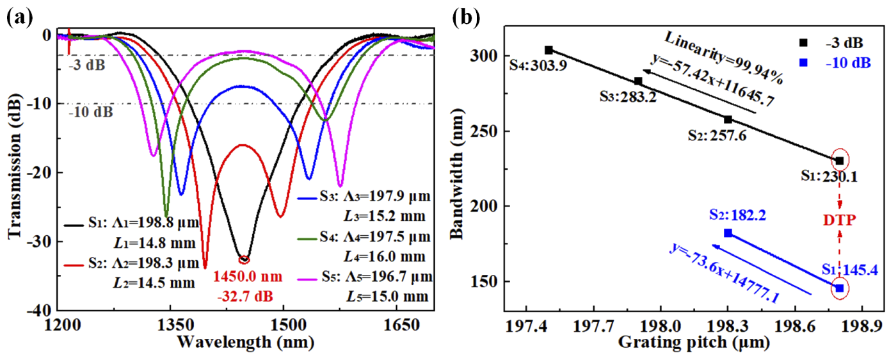

Fig. 4. (a) Transmission spectra of five prepared HLPFGs (S_1-S_5) with decreasing grating pitch Λ. (b) Measured −3 dB and −10 dB bandwidth versus the grating pitch Λ.

3.2. OAM mode characterization

The phase property of the generated OAM mode is characterized by employing a tunable laser source (1450–1650 nm) and the aforementioned MZI observation system. The HLPFG S_2 is employed for observation and both the mode field and interference field is shown in Fig. 5(b). Within the wavelength range of 1450–1540 nm, OAM mode with a topological charge number of 1 is clearly observed, convincing the generation of broadband OAM mode. Unfortunately, limited by the wavelength range (1450–1650 nm) of the employed tunable laser, the interference field as well as the mode field distribution at a shorter wavelength range of 1357.4–1450 nm is not measured in the experiment. While, according to the transmission spectra evolution with the grating pitch Λ that shown in Fig. 4(a), together with the calculated dispersion relationships that shown in Fig. 1, the mode at wavelength of 1357.4–1450 nm is convinced as the same $LP_{1,10}$ mode. As such, the mode properties within 1357.4–1450 nm will be all the same as observed in Fig. 5(b). As observed in Fig. 5(a), the OAM mode bandwidth of S_2 is 257.6 nm @ −3 dB and 182.2 nm @ −10 dB, respectively. It is worth noting that, the bandwidth of generated OAM mode can be broadened further by reducing the grating pitch Λ further, at the cost of OAM

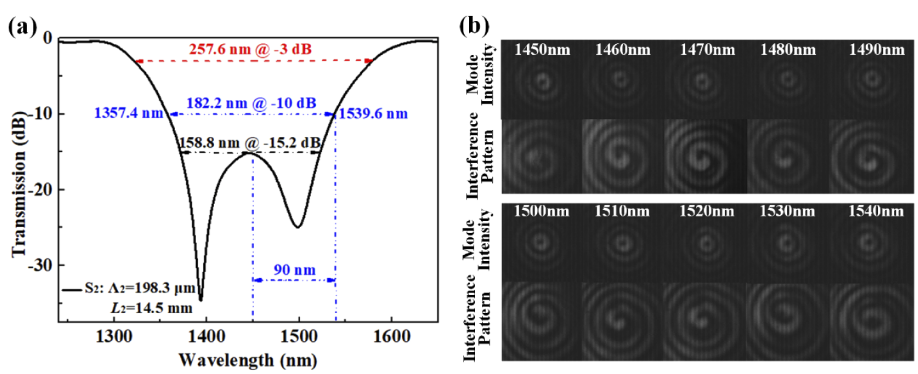

Fig. 5. (a) Transmission spectrum of a prepared HLPFG (S_2) with grating pitch Λ of 198.3 μm; (b) Measured mode field distribution and interference patterns within the broadband resonant dip (from 1450 to 1540 nm).

Optics EXPRESS

mode conversion efficiency. As shown in Fig. 4(a), a broader OAM mode bandwidth renders a shallower resonant dip, i.e. a lower conversion efficiency. To our best knowledge, this is the first experimental demonstration of broadband OAM mode generation based on a conventional SMF and oxyhydrogen-flame approach.

4. Dynamical tunability of the OAM mode

4.1. Wavelength and bandwidth tunability by torsion

As described above, precise controlling of the grating pitch Λ is crucial to the OAM mode bandwidth. Alternatively, we find a more flexible and convenient way to tuning the bandwidth of the OAM mode dynamically, i.e. twisting the prepared HLPFG. The twisting equipment is schematically depicted in Fig. 6, where the two pigtails of the prepared HLPFG are fixed to a rotation stage and a stationary stage by a pair of fiber holders, respectively. The pigtails of the HLPFG are connected to a supercontinuum light source and Optical Spectrum Analyzer (OSA), respectively, to monitor the transmission spectra of the HLPFG during the twisting. The two HLPFGs (S_1 and S_2) are twisted from 0 to 360° (CW) and −360° (CCW) with a step of 60°, respectively. At each step, the transmission spectra are recorded and plotted in Fig. 7(a) and 8(a), respectively. All the tests are performed in a stable room temperature of 25 °C. It is worth noting that the CW direction is defined as the helix directions of the HLPFG while the CCW direction is opposite. A twist rate parameter γ that defined as

$$\gamma = \pi\theta/180L' \tag{4}$$

is employed to quantitatively characterize the twist-induced stress per unit length. Here, θ and $L' = 12.6$ cm are the twisting angle and the fiber length between the two fiber holders, respectively.

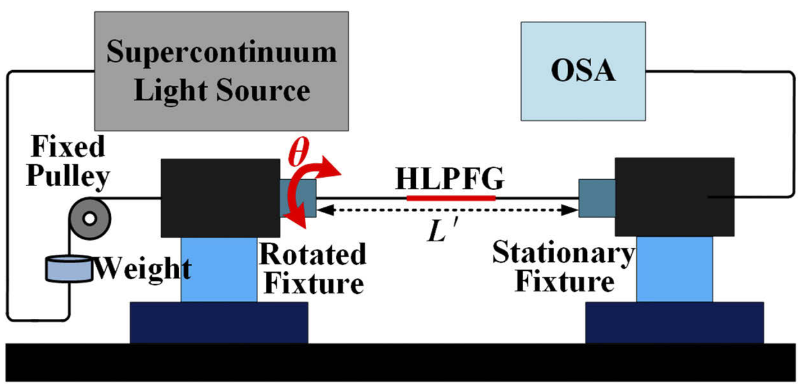

Fig. 6. Schematic diagram of the twisting setup.

The blackline in Fig. 7(a) is the initial transmission spectrum of S_1. With the increasing of θ in the CW direction (the helix direction of HLPFG), the single resonant dip splits and shift toward the opposite directions, rendering a wider OAM mode bandwidth at both −3 and −10 dB. While, the resonance gets shallower when twisting the HLPFG in the CCW direction (opposite to the HLPFG helix). The −3 dB and −10 dB bandwidth of the OAM mode versus the twist rate γ in both CW and CCW directions are shown in Fig. 7(b), where the −3 dB and −10 dB bandwidth can be dynamically tunned from 210.1 and 102.1 nm to 260.4 and 182.8 nm, respectively. For S_2, the experimental results are presented in Fig. 8, where the −3 dB and −10 dB bandwidth can be tuned from 235.7 nm and 148.0 nm to 280.7 nm and 207.5 nm, respectively.

Optics EXPRESS

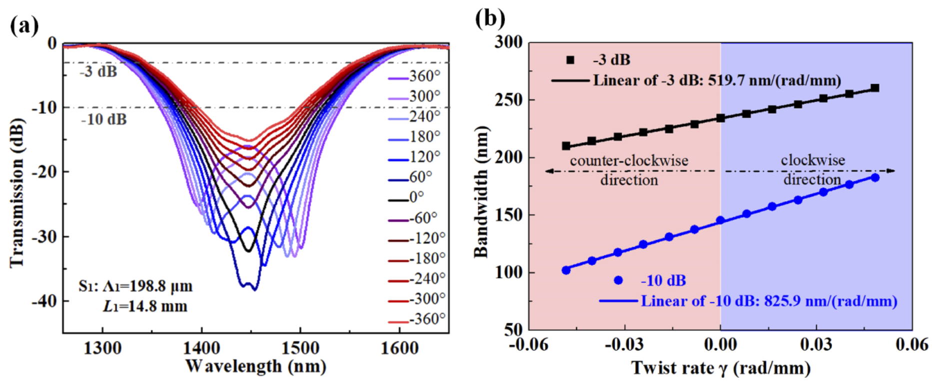

Fig. 7. (a) Evolution of the transmission spectrum of S_1 with varying torsion angles. (b) The −3 dB and −10 dB bandwidth of OAM mode versus the twist rate γ.

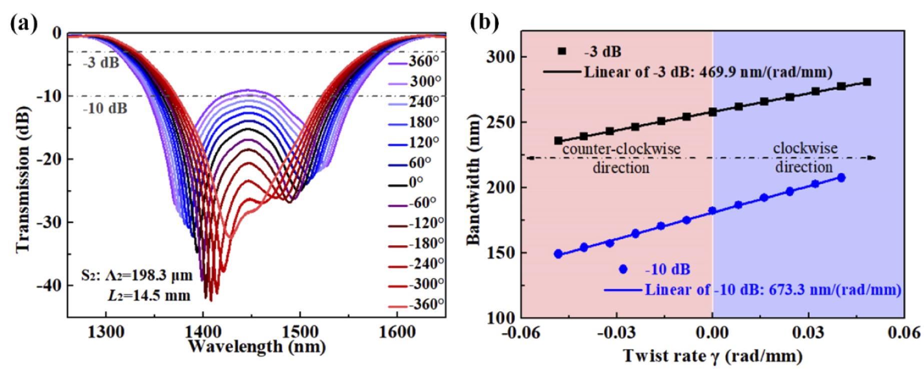

Fig. 8. (a) Evolution of the transmission spectrum of S_2 with varying torsion angles. (b) The −3 dB and −10 dB bandwidth of OAM mode versus the twist rate γ.

Table 1. Comparison of several all-fiber OAM mode converters

Structure	Fiber type	Method	Bandwidth	Tunability	Year	Reference
Apodised LPFG	FMF	Etching	300 nm @−10 dB	No	2017	[23]
Phase-shifted LPFG	FMF	CO_2 laser	182 nm @−10 dB	No	2019	[24]
LPFG	FMF	CO_2 laser	156.4 nm @−10 dB	No	2019	[16]
HLPFG	SMF	Simulation	287nm@−3 dB	No	2020	[22]
HLPFG	**SMF**	**Oxyhydrogen-flame**	**303.9 nm @−3 dB** **182.2 nm @−10 dB** **158.8 nm @−15.2 dB**	**Yes**	**This work**	

4.2. Discussion

Here, two points are worth noting. Firstly, by twisting the HLPFG with a larger angle θ or further reducing the L', the bandwidth of OAM mode can be tuned in a wider range. The principle of torsion tunability can be considered to a combined effect of grating pitch changing and the photo-elastic effect, which together brings about the wavelength and bandwidth change. Secondly, the mode field images of the OAM mode of S_1 and S_2 didn't given repeatedly since the mode fields have been detailed analyzed in the previous section. As such, the dynamical tunability of the bandwidth of the OAM mode is verified.

Table 1 displays some typical results from previously reported all-fiber OAM mode converters. Compared with other types of all-fiber OAM mode converter, the oxyhydrogen-flame-induced HLPFG in this work has a simple structure, a broader bandwidth and a dynamic tunability of bandwidth.

5. Conclusion

We proposed and demonstrated a new approach for broadband tunable OAM mode generation based on oxyhydrogen-flame-induced HLPFG in a conventional SMF. The -3 dB and -10 dB bandwidth of the OAM mode are 303.9 nm and 182.2 nm, respectively. The dynamical tunability of the bandwidth is also reported. The proposed method and device may find vital applications in large-capacity optical fiber communications systems.

Funding. National Key Research and Development Program of China (2018YFF01010202); National Natural Science Foundation of China (61905164, 61905165); China Postdoctoral Science Foundation (2020M683184); Chongqing Municipal Education Commission (KJZD-M2000602); Natural Science Foundation of Guangdong Province (2018KQNCX219).

Disclosures. The authors declare no conflicts of interest.

Data Availability. The datasets are available from the corresponding author on reasonable request

References

1. B. Mukherjee, "WDM optical communication networks: progress and challenges," IEEE J. Select. Areas Commun. **18**(10), 1810–1824 (2000).
2. P. Sillard, D. Molin, M. Bigot-Astruc, A. Amezcua-Correa, K. D. Jongh, and F. Achten, "50 µm multimode fibers for mode division multiplexing," J. Lightwave Technol. **34**(8), 1672–1677 (2016).
3. D. J. Richardson, J. M. Fini, and L. E. Nelson, "Space-division multiplexing in optical fibers," Nat. Photonics **7**(5), 354–362 (2013).
4. N. Bozinovic, Y. Yue, Y. Ren, M. Tur, P. Kristensen, H. Huang, A. E. Willner, and S. Ramachandran, "Terabit-Scale Orbital Angular Momentum Mode Division Multiplexing in Fibers," Science **340**(6140), 1545–1548 (2013).
5. S. Yijie, X. Wang, Z. Xie, C. Min, and X. Yuan, "Optical vortices 30 years on: oam manipulation from topological charge to multiple singularities," Light: Sci. Appl. **8**(1), 1–29 (2019).
6. L. Yan, P. Gregg, E. Karimi, A. Rubano, L. Marrucci, R. Boyd, and S. Ramachandran, "Q-plate enabled spectrally diverse orbital-angular-momentum conversion for stimulated emission depletion microscopy," Optica **2**(10), 900–9033 (2015).
7. V. Kotlyar, A. Kovalev, A. Porfirev, and E. Kozlova, "Orbital angular momentum of a laser beam behind an off-axis spiral phase plate," Opt. Lett. **44**(15), 3673–3676 (2019).
8. H. Zhou, S. Fu, Y. Zhai, C. Yin, and C. Gao, "Spatial light modulator-based programmable j-plate for the arbitrary spin-to-orbital angular momentum conversion of lights," Appl. Phys. B **125**(3), 42 (2019).
9. S. Slussarenko, A. Murauski, T. Du, V. Chigrinov, and E. Santamato, "Tunable liquid crystal q-plates with arbitrary topological charge," Opt. Express **19**(5), 4085–4090 (2011).
10. S. Chen, Y. Cai, G. Li, S. Zhang, and K. W. Cheah, "Geometric metasurface fork gratings for vortex-beam generation and manipulation," Laser Photonics Rev. **10**(2), 322–326 (2016).
11. S. Oh, K. R. Lee, U. C. Paek, and Y. Chung, "Fabrication of helical long-period fiber gratings by use of a CO_2 laser," Opt. Lett. **29**(13), 1464–1466 (2004).
12. K. Ren, L. Ren, J. Liang, X. Kong, H. Ju, and Z. Wu, "Online and efficient fabrication of helical long-period fiber gratings," IEEE Photonics Technol. Lett. **29**(14), 1175–1178 (2017).
13. Z. Bai, Y. Wang, Y. Zhang, C. Fu, and J. He, "Helical long-period fiber gratings as wavelength-tunable orbital angular momentum mode generators," IEEE Photonics Technol. Lett. **32**(7), 418–421 (2020).
14. H. Li, P. Wang, and H. Zhao, "All-fiber second-order orbital angular momentum generator based on a single-helix helical fiber grating," Opt. Lett. **44**(21), 5370–5373 (2019).

Optics EXPRESS

15. X. Zhao, Y. Liu, Z. Liu, and C. Mou, "All-fiber bandwidth tunable ultra-broadband mode converters based on long-period fiber gratings and helical long-period gratings," Opt. Express **28**(8), 11990–12000 (2020).
16. Y. Guo, Y. G. Liu, Z. Wang, H. Zhang, and Z. Li, "More than 110-nm broadband mode converter based on dual-resonance coupling mechanism in long period fiber gratings," Opt. Laser Technol. **118**, 8–12 (2019).
17. C. Jiang, Y. Liu, Y. Zhao, L. Zhang, C. Mou, and T. Wang, "Helical Long-period Fiber Grating Written in Polarization-maintaining Fiber by CO_2-laser," *CLEO, OSA Technical Digest* (online). paper SM2 K.2 (2018).
18. G. K. L. Wong, M. S. Kang, H. W. Lee, F. Biancatana, C. Conti, T. Weiss, and P. St. J. Russell, "Excitation of orbital angular momentum resonances in helically twisted photonic crystal fiber," Science **337**(6093), 446–449 (2012).
19. B. Sun, W. Wei, C. Liao, L. Zhang, Z. Zhang, M. Chen, and Y. Wang, "Automatic arc discharge-induced helical long period fiber gratings and its sensing applications," IEEE Photonics Technol. Lett. **29**(11), 873–876 (2017).
20. Z. Li, S. Liu, Z. Bai, C. Fu, Y. Zhang, Z. Sun, X. Liu, and Y. Wang, "Residual-stress-induced helical long period fiber gratings for sensing applications," Opt. Express **26**(18), 24114–24123 (2018).
21. L. Y. Ren, K. L. Ren, J. Liang, L. Yang, and W. Zhang, "Excitation of high-quality orbital angular momentum vortex beam in adiabatically helical twisted single-mode fiber," Opt. Express **29**(6), 8441–8450 (2021).
22. K. L. Ren, M. H. Cheng, L. Y. Ren, Y. H. Jiang, D. D. Han, Y. K. Wang, J. Dong, J. H. Liu, L. Yang, and Z. Q. Xi, "Ultra-broadband conversion of OAM mode near the dispersion turning point in helical fiber gratings," OSA Continuum **3**(1), 77–87 (2020).
23. W. Wang, J. Wu, K. Chen, W. Jin, and K. Chiang, "Ultra-broadband mode converters based on length-apodized long-period waveguide gratings," Opt. Express **25**(13), 14341–14350 (2017).
24. Y. Zhao, Z. Liu, Y. Liu, C. Mou, T. Wang, and Y. Yang, "Ultra-broadband fiber mode converter based on apodized phase-shifted long-period gratings," Opt. Lett. **44**(24), 5905–5908 (2019).